

2022

Modeling and Simulation of Air-Source CO₂ Heat Pump Water Heater

Zhiming Gao

Keith Rice

Kashif Nawaz

Follow this and additional works at: <https://docs.lib.purdue.edu/iracc>

Gao, Zhiming; Rice, Keith; and Nawaz, Kashif, "Modeling and Simulation of Air-Source CO₂ Heat Pump Water Heater" (2022). *International Refrigeration and Air Conditioning Conference*. Paper 2361.
<https://docs.lib.purdue.edu/iracc/2361>

This document has been made available through Purdue e-Pubs, a service of the Purdue University Libraries. Please contact epubs@purdue.edu for additional information. Complete proceedings may be acquired in print and on CD-ROM directly from the Ray W. Herrick Laboratories at <https://engineering.purdue.edu/Herrick/Events/orderlit.html>

Modeling and Simulation of Air-Source CO₂ Heat Pump Water Heater

Zhiming Gao*, Keith Rice, Kashif Nawaz

Oak Ridge national laboratory

*Corresponding author (gaoz@ornl.gov, 865-241-5018)

ABSTRACT

Carbon dioxide (CO₂) has been widely used as working fluid for the vapor-compression refrigeration systems in large marine device. Due to the potential energy efficiency and the favorable environmental properties of CO₂ as a working fluid, CO₂ heat pump water heater (HPWH) systems are regarded a promising technology for centralized domestic hot water (DHW) heating in residential and commercial buildings. However, it is still at the early stage of appropriately optimizing and improving the energy performance of CO₂ HPWH. This requires CO₂ HPWH simulation tools capable of capturing the accurate impact of the emerging compressor, throttle device, and heat exchanger technology on CO₂ heat transfer and energy efficiency. In this study, high efficiency components (compressors, pumps, fans, heat exchangers) were identified and applied to the state-of-art CO₂ HPWH designs and analyzed their performance by using numerical simulation. This was done by simulating the performance of CO₂ HPWH using ACMODEL design model combined with the component models developed at Oak Ridge National Laboratory (ORNL) for orifice tube, map-based compressor, and tube-in-tube gas cooler. The simulated CO₂ HPWH performance was then compared with the heat pump water heater using conventional refrigerants. The results reflected that the current CO₂ HPWH component and system technology achieved a lower uniform energy factor in the application of U.S. residential hot water supply not exceeding 140°F. It is vital for CO₂ HPWHs to continuously improve compressor and system efficiency via novel component design.

1. INTRODUCTION

Carbon dioxide (CO₂) is used as working fluid in large marine vapor-compression refrigeration device. A typical CO₂ transcritical vapor compression cycle consists of at least four components: a compressor to lift the pressure of the fluid from evaporating pressure to heat rejection pressure, a “gas cooler” to reject heat to the environment, an expansion device to reduce the pressure of the fluid to evaporating pressure, and an evaporator to absorb heat from the conditioned space (Ortiz et.al., 2003). Beyond these basic components mentioned above, extra components may be added to control the system’s operation or to improve system efficiency. Since 1990s, CO₂ has been extensively investigated as alternative refrigerant for residential air conditioning/heat pump and heat pump water heater in order to deal with global warming and ozone depletion (Kim et.al., 2004).

The results from a large number of thermodynamic analyses have been reported that the theoretical efficiency of CO₂ cycles is much less than R134a and R410a while CO₂ volumetric refrigeration capacity is 3-10 times larger than R134a and R410a (Kim et. al., 2004, Groll et. al., 2007). However, higher vapor density in a CO₂ transcritical cycle can improve compressor volume efficiency and generate more homogenous two-phase flow. Moreover, the available results for evaporative heat transfer have indicated that CO₂ achieves 50% better heat transfer coefficient and 70%-80% lower pressure drop than R22 and R410a (Park et. al., 2007). Similarly, the heat transfer coefficients of CO₂ gas cooling are also better than the condensation heat transfer coefficients of the conventional refrigerants at the identical operating conditions (Cheng et. al., 2008). Thus the actual performance of CO₂ substantially depends on system optimization and emerging technologies, as well as the constraints of operation conditions.

The experimental results from CO₂ heat pump system demonstrated that the CO₂ system achieved lower heating and cooling cycle-COP with higher capacity compared to R410a or R22 heat pump systems, except at low ambient temperatures in heating mode. A prototype CO₂ system was tested in 2002 and showed that the cooling COP of the CO₂ unit was much lower than the R22 unit (Nekså, 2002). This study, however, also pointed out the heating COP of the CO₂ unit was slightly higher than the R22 unit at low ambient temperatures, but the overall result could be a significant increase in space heating energy efficiency for the CO₂ system owing to a lower need for supplementary electrical heating. A similar result was reported in 2003 and confirmed that the CO₂ heat pump system designed to match the packaging constraints of an R410a heat pump system was able to achieve less heating COP and greater capacity except at low outdoor temperature (Richter et. al., 2003). The studies in 2006 further compared the latest-generation prototype CO₂ split type heat pump unit with the most energy-efficient Japanese R410a split-type heat pump unit available on the market. The tests were carried out at two different climates. The results show that the heating seasonal performance factor (HSPF) for the CO₂ was about 3%-7% higher than that of R410a in heating

mode, but the seasonal energy efficiency ratio (SEER) of the CO₂ unit in cooling mode could be 17 % less than that of the R410a unit (Jakobsen et.al., 2006).

Compared to CO₂ air conditioning or heat pump systems, the reported cases have shown a good potential of energy saving for CO₂ heat pump water heater (HPWH) (Nawaz, 2018, He 2020, Ye 2020). A CO₂ heat pump water heater can heat water through using supercritical CO₂ and efficiently can raise water from low to high temperature in a single-stage compressor cycle. Supercritical CO₂ does not experience phase change, thus the temperature of CO₂ drops gradually as the water is heated. Usually, conventional refrigerants have to use high condensing temperature to heat up low-temperature water instead, leading to irreversible heat loss and low performance. Thus, as a refrigerant, CO₂ is more appropriate for water heating application with large temperature lifting. The study of CO₂ heat pump water heater was initiated at SINTEF/NTNU from the late 1980s (Nekså et.al, 1998), and the results from extensive measurements at a 50kW-heating-capacity prototype showed that a COP above 4 was achieved even for a hot water temperature of 140 °F. The energy consumption can be reduced by 75% compared to electrical or gas fired systems. Hwang and Radermacher (1998) theoretically compared the performance of R22 and CO₂ for water-heating applications, and concluded that CO₂ heat pump water heating was approximately 10% better than R22 across a wide range of ambient temperatures. Other literatures shows that a CO₂ heat pump water heater can produce hot water with temperature up to 194 °F without operational problem and with only a small loss in efficiency (Kim et.al., 2004). Stene (2005) developed a residential CO₂ vapor compression system combining space heating and hot water heating. His experimental results illustrates that a CO₂ heat pump system achieves the same or higher seasonal performance factor (SPF) than the most energy efficient state-of-the-art heat pump systems as long as: (1) the heating demand for hot water production constitutes at least 25% of the total annual heating demand of the residence, (2) the return temperature in the space heating system is about 86 °F or lower, (3) the city water temperature is about 50 °F or lower. Air-to-water and water-to-water CO₂ HPWH systems in the capacity range from about 5 to 60 kW are now available in Japan and Europe from a few of manufacturers.

Due to potential energy efficiency and the favorable environmental properties of CO₂ as a working fluid, CO₂ heat pump water heater systems are regarded a promising technology for centralized domestic hot water (DHW) heating in residential and commercial buildings. However, there are few examples of appropriately evaluating the options improving uniform energy factor (UEF) of CO₂ heat pump water heater on the US market in the literatures. This is due, in part, to lack of CO₂ heat pump water heater simulation tools capable of capturing the accurate impact of the emerging compressor, throttle device, and heat exchanger technology on CO₂ heat transfer and energy efficiency. In this study, high efficiency components (compressors, pumps, fans, heat exchangers) were identified and applied to the current CO₂ HPWH designs and analyzed their UEFs by using numerical simulation. This was done by simulating the performance of CO₂ heat pump water heater using ACMODEL design model combined with orifice tube, map-based compressor, and tube-in-tube gas cooler component models developed at Oak Ridge National Laboratory (ORNL). ACMODEL is an equipment design model for CO₂-based air conditioners and heat pumps developed by Purdue University to account for the details of each component (Ortiz et.al., 2003). The CO₂ system performance maps were then input to TRNSYS models for the analysis of UEF. In the following section, the details of the methodology are explained.

2. HPWH simulation model

A number of simulation models have been developed to predict steady-state CO₂ vapor compression cycle. These models are classified into simple thermodynamics models (Liao et.al., 2000, Fartaj et.al., 2004, Yang et.al., 2005) and the low-order phenomenological models Rigola et.al., 2005, Ortiz et.al., 2003). The thermodynamics models are essentially based on the first and second laws of thermodynamics to conduct parametric studies on the transcritical carbon dioxide refrigeration cycles. They were used to identify the thermodynamic mechanism of CO₂ vapor compression cycle, but not enough to fully understand the performance of CO₂ system. The low-order phenomenological models reasonably consider the effect of heat transfer, realistic component geometry and behavior on the performance of CO₂ system. Thus, the low-order phenomenological CO₂ models are able to better predict and design the performance of CO₂ system. For example, ACMODEL developed by Purdue University were used to account for the geometry of each heat exchanger; the type (hermetic or open-drive), volume, speed and efficiency of the compressor; the type (isenthalpic or work-producing) and efficiency of the expander; and other necessary components. The simulation package has been widely applied by Groll and his coworkers in simulating CO₂ air conditioners (Ortiz et.al., 2003, Li et.al., 2005, Liu et.al., 2008). However, these models are still insufficient to evaluate the CO₂ heat pump water heater design, as mentioned above. This paper reports a simulation model for CO₂ heat pump water heater based on updating ACMODEL with the additional component models of emerging

compressor, water-to-CO₂ heat exchanger, microchannel evaporator, and expansion device. The key component models are described below.

2.1 Compressor

The compression process is defined based on a simple approach of using compression efficiency and volumetric efficiency to correct the ideal compression process. These efficiencies are considered as functions of compressor discharge pressure and pressure ratio.

$$\eta_{is} = \frac{\dot{W}_{CO_2, isentropic}}{\dot{W}_{CO_2}} = \frac{\dot{m}_{CO_2} (h_{discharge, isentropic} - h_{suction})}{\dot{W}_{CO_2}} \quad (1)$$

$$\begin{aligned} &= a_1 + a_2 P_d + a_3 P_d^2 + a_4 Pr + a_5 Pr^2 + a_6 P_d Pr \\ \eta_v &= \frac{\dot{m}_{CO_2}}{\dot{m}_{CO_2, theoretical}} = \frac{\dot{m}_{CO_2}}{RPM \cdot V_{displacement} \cdot \rho_{suction}} \quad (2) \\ &= b_1 + b_2 P_d + b_3 P_d^2 + b_4 (1 - Pr) + b_5 (1 - Pr)^2 + b_6 P_d (1 - Pr) \end{aligned}$$

where η_{is} is isentropic efficiency; η_v is volumetric efficiency; P_d is compression discharge pressure; Pr is the pressure ratio of compression process; $h_{discharge, isentropic}$ is discharge enthalpy at ideal compression; $h_{suction}$ is enthalpy at suction line; $V_{displacement}$ is compressor displacement; $\rho_{suction}$ is density at suction line; \dot{W}_{CO_2} is CO₂ compression power consumption; \dot{m}_{CO_2} is CO₂ mass flow rate. The efficiencies are used to calculate \dot{m}_{CO_2} and \dot{W}_{CO_2} .

Table 1 The parameters used in Eqs. (1)-(2).

i	a_i	b_i
1	8.92831251E-01	1.62057438E+00
2	-5.54602580E-04	-8.82693649E-04
3	1.37908840E-07	2.26374783E-07
4	4.89701570E-02	-8.36998637E-02
5	-1.05806466E-02	-3.39793735E-03
6	1.98432624E-05	3.93938644E-05

The coefficients used in Eqs. (1) and (2) are listed in Table 1. These values are directly estimated by fitting OEM compressor technical data. The compressor is a reciprocating model designed for use with CO₂ with 0.107 in³ (1.75 cm³) displacement, nominal 220V, and 60 Hz frequency.

The enthalpy at the exit of the entire compressor is further refined as Eq. 3 to account for heat loss of the compressor.

$$h_{discharge} = h_{suction} + \frac{(1 - \eta_{loss}) \dot{W}_{CO_2}}{\dot{m}_{CO_2}} \quad (3)$$

where η_{loss} (= 0.45) is compressor heat loss ratio; $h_{discharge}$ is CO₂ discharge enthalpy at compression process. The assumptions for this compressor shell heat loss were obtained from the manufacturer which provided measured discharge temperatures, from which the shell heat loss levels were calculated over the range of condensing temperatures.

2.2 Water-to-CO₂ Heat Exchanger

The water-to-CO₂ heat exchanger is considered as a counterflow tube-in-tube heat exchanger. CO₂ moves within inner tube while water is in opposition to go through annulus tube (shown in figure 1). Both inner and annulus tubes are assumed to be smooth tubes, and CO₂ is assumed to be homogeneous and supercritical state. The model accounts for energy conservation and heat transfer between CO₂ and water flow. Briefly, the volume of the water-to-CO₂ heat exchanger is divided into multi-segment. The calculation of each segment is iterated until the given variables are equal to the variables calculated by the LMTD method. The simulation of the heat exchanger model requires CO₂

enthalpy and pressure at the inlet, as well as water inlet and outlet temperature of this heat exchanger. Other required parameters include carbon dioxide mass flow rate as well as the geometry of the heat exchanger. Key features of the component model follow.

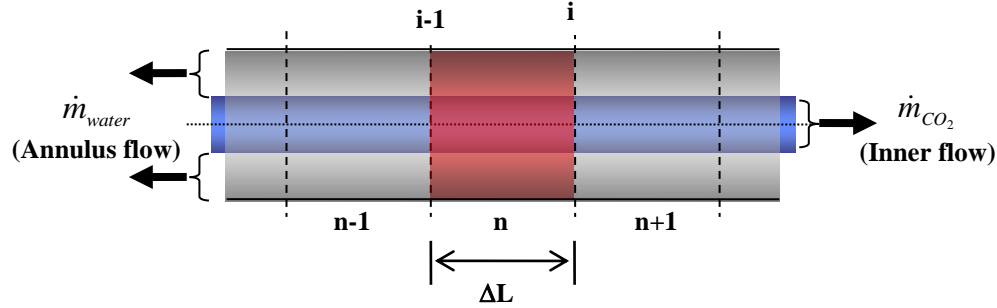


Figure 1 Scheme of single segment in the water-to-CO₂ heat exchanger.

The equation for the overall heat transfer rate in each segment is described as below.

$$\dot{Q}_{NTU} = \varepsilon c_{\min} (T_{CO_2, in} - T_{wat, in}) \quad (4)$$

where c_{\min} is the minimum thermal capacitance of $\dot{m}_{CO_2} C_{P_{CO_2}}$ and $\dot{m}_{wat} C_{P_{wat}}$; ε is the heat exchanger effectiveness; $T_{CO_2, in}$ is CO₂ inlet temperature; $T_{wat, in}$ is water inlet temperature.

The equation of ε for a counterflow heat exchanger is given as

$$\varepsilon = \frac{1 - \exp[-NTU(1 - c_r)]}{1 - c_r \exp[-NTU(1 - c_r)]} \quad (5)$$

where $c_r = c_{\min} / c_{\max}$; $NTU = UA / c_{\min}$; UA is the overall heat transfer conductance which is followed.

$$UA = \frac{1}{\frac{1}{(hA)_{CO_2}} + \frac{\ln(r_o/r_i)}{2\pi k \Delta L} + \frac{1}{(hA)_{wat}}} \quad (6)$$

Here r_o and r_i are outside and inside radii of inner tube, respectively; k is the tube thermal conductivity; ΔL is segment length; $(hA)_{CO_2}$ and $(hA)_{wat}$ are the CO₂-side and water-side overall heat transfer conductance, respectively.

Meanwhile, the overall heat transfer rate is expressed by using heat transfer and energy conservation in the inner tube and annulus tube, as follows.

$$\dot{Q}_{NTU} = \dot{Q}_{UA_{CO_2}} = \dot{Q}_{UA_{wat}} = \dot{Q}_{CO_2} = \dot{Q}_{wat} \quad (7a)$$

$$\dot{Q}_{UA_{CO_2}} = (hA)_{CO_2} (\bar{T}_{CO_2} - T_{wall_CO_2}) \quad (7b)$$

$$\dot{Q}_{UA_{wat}} = (hA)_{wat} (T_{wall_wat} - \bar{T}_{wat}) \quad (7c)$$

$$\dot{Q}_{CO_2} = \dot{m}_{CO_2} (h_{CO_2, in} - h_{CO_2, out}) \quad (7d)$$

$$\dot{Q}_{wat} = \dot{m}_{wat} (h_{wat, out} - h_{wat, in}) \quad (7e)$$

The heat transfer rate predicted by Eq. (4) and Eq. (7) are required to match in an effort of numerical convergence. \bar{T}_{CO_2} , \bar{T}_{wat} , $T_{wall_CO_2}$, and T_{wall_wat} are the average CO₂ temperature, average water temperature, average wall temperature at CO₂ side, and average wall temperature at water side, respectively. The segment CO₂-side and water-side outlet temperatures are estimated based on water and CO₂ energy conservation (see Eqs. (7d)- (7e), respectively). The segment CO₂-side and water-side inlet and outlet temperatures are used to estimate the average CO₂ temperature and average water temperature. In the above equations, single-phase refrigerant-side heat transfer coefficient is calculated using the modified Gnielinski correlation. Water-side heat transfer coefficient is computed using Dittus-Boelter correlation.

CO₂ pressure drop in the counterflow tube-in-tube heat exchanger accounts for pressure loss (ΔP_i) at the entrance to the inner tube, pressure loss (ΔP_f) due to frictional loss, pressure change (ΔP_c) due to compressibility effects, and pressure loss (ΔP_e) associated with expansion of flow at the exit of the inner tube. They are described as:

$$\Delta P = \Delta P_i + \Delta P_f + \Delta P_c + \Delta P_e \quad (8a)$$

$$\Delta P_i = \frac{1}{2} K_i \rho_{CO_2} V_{CO_2}^2 \quad (8a)$$

$$\Delta P_f = f \frac{L}{2d} \rho_{CO_2} V_{CO_2}^2 \quad (8b)$$

$$\Delta P_c = \dot{m}_{CO_2}^2 \left(\frac{1}{\rho_{CO_2,out}} - \frac{1}{\rho_{CO_2,in}} \right) \quad (8c)$$

$$\Delta P_e = \frac{1}{2} K_e \rho_{CO_2} V_{CO_2}^2 \quad (8d)$$

where K_i is CO₂ entrance loss coefficient; K_e is CO₂ exit loss coefficient; d is the diameter of inner tube; f is the friction factor for supercritical CO₂ in inner tube; f is estimated by using the Kuraeva and Protopopov correlation (see Ortiz et. al., 2003). \dot{m}_{CO_2} is CO₂ mass flow rate. V_{CO_2} is CO₂ volume flow rate; ρ_{CO_2} is CO₂ density.

The above heat transfer coefficient and friction factor for CO₂ in the heat exchanger are calculated in the same manner as used for the gas-cooler which is described in (Ortiz et. al., 2003). Water-side heat transfer coefficient is calculated using Dittus-Boelter correlation (Dittus et. al., 1930). The power consumption of water pump, \dot{W}_{pump} , is calculated by using an empirical correlation, which is considered as a function of water mass flow rate:

$$\dot{W}_{pump} = 0.1427 \cdot \dot{m}_{wat} \quad (9)$$

In the equation, the unit of power consumption is kilowatt. \dot{m}_{wat} is the water mass flow rate (kg/s).

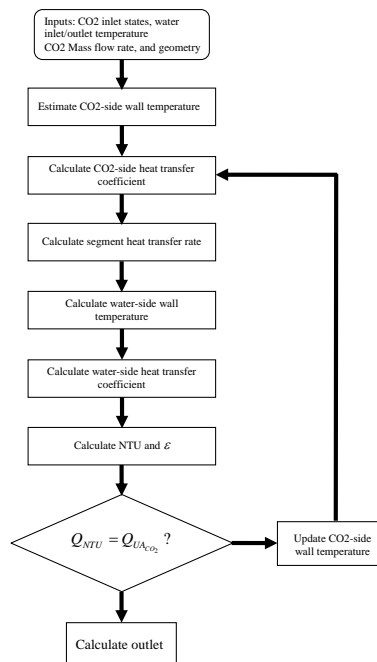


Figure 2 Control diagram of single volume segment for water-to-CO₂ heat exchanger.

The numerical procedure for water-to-CO₂ heat exchanger follows the same methodology presented by Ortiz et. Al. (2003). The calculation of this counterflow tube-in-tube heat exchanger starts at volume segments and thermal temperature initialization. In each volume segment, the CO₂-side wall temperature in the inner tube is then estimated as a linear interpolation of CO₂ and water inlet temperatures. Thus CO₂-side heat transfer coefficient and segment heat transfer rate are computed based on the estimated wall temperature. Then, the water-side wall temperature of inner tube is evaluated by using the segment heat transfer rate, CO₂ inlet temperature, and the inner-tube thermal conductance. The water-side heat transfer coefficient is also calculated. Then, the segment CO₂-side and water-side outlet temperatures are calculated. After that, the number of transfer units (NTU) and heat exchanger effectiveness (ϵ) are calculated and Ridders' method is used to seek the correct value of the inside-wall temperature of inner tube, which allows Equations (3) and (6b) to achieve the same value of segment heat transfer rate. Finally, the segment CO₂-side pressure drops are calculated. This procedure is illustrated in Figure 2.

2.3 Evaporator

The evaporator module provided in the ACMODEL code is directly used to predict evaporation behavior. The module accounts for wet-surface air-side heat transfer and two-phase refrigerant-side heat transfer process in the code. In the methodology, the evaporator volume is also divided into multiple segments. Briefly, air-side heat transfer coefficients and friction factors for dry volume segments in the evaporator are treated using the Chang et al. correlation (1994); air-side dry surface friction factors are calculated using the accompanying Chang et al. correlation (1994); wet surface friction factors are calculated using the Wang et al. correlation (2000). Two-phase refrigerant-side heat transfer coefficients are calculated according to the Kandlikar correlation (1990). Single-phase refrigerant-side heat transfer coefficients are calculated according to the modified Gnielinski correlation (Pettersen et.al., 2000). Two-phase refrigerant-side friction factors are calculated using the Churchill correlation (Yin et.al., 2001) with the Reynolds number evaluated using a homogeneous two-phase density and viscosity. Single phase refrigerant friction factors are calculated using the Churchill correlation with a single-phase Reynolds number. Permissible evaporator states are subcooled, two-phase or superheated. In the simulation, the evaporator is considered as a louvered-fin heat exchanger with microchannel.

2.4 Expansion device

The expansion device is assumed as isenthalpic expansion process with negligible kinetic and potential energy changes. The expansion device in the simulation model uses the literature model (Chen et.al., 2004) to balance refrigerant pressure level and mass flow rate between compressor and expansion device. The model claimed that approximately 95% of the measured data were within $\pm 6\%$. The flow mass rate control is described as follows.

$$\dot{m}_{CO_2} = A_s \sqrt{2\rho_{up}(P_{up} - P_f)} \quad (10)$$

$$P_f = P_c \left(1.17344 + 0.0306D_R^{3.70318} - 0.37139P_R^{-4.29588}T_R^{0.03813} + 0.00002\left(\frac{L}{D}\right)^{2.13404} \right) \quad (11)$$

where ρ_{up} is upstream CO₂ density; P_{up} is upstream pressure; P_f is downstream pressure; P_c is critical pressure; $P_R = P_{up}/P_c$; A_s is cross-sectional area of the short tube; D_R is normalized diameter (D/D_{ref}). $T_R = (T_{up} - T_c)/T_c$; L is tube length; D is tube diameter; D_{ref} is referenced diameter; T_{up} is upstream temperature; T_c is critical temperature.

3. SIMULATION CONDITIONS AND RESULTS

To evaluate the potential of a residential CO₂ HPWH designed under US residential application standards, it is important to design an appropriate CO₂ HPWH by referring to the size and auxiliary components of an efficient HPWH commercially available. Thus, a residential R410A HPWH available in US market is considered as a benchmark equipment (Gao et.al. 2003, Gao. 2010), which is equipped with a high-efficiency rotary compressor, a water-to-refrigerant condenser, a finned tube evaporative heat exchanger, and TXV device, as well as water pump and air fan (Baxter et.al. 2011). The compressor with the displacement of 0.33 in³ has 4850 Btu/hr cooling capacity rated at 45 °F Te/130 °F Tc/20 °F SH/15 °F SC. The water-to-refrigerant condenser is a counterflow Packless double-walled fluted tube heat exchanger with a size to give a relatively low mean condensing temperature difference of about 9°F for the R-410A case at 115°F entering water temperature (EWT). The water pump used in the condenser is a brushless permanent magnet motor (BPM) with the pump flow to be optimized for each design for an assumed

system head curve. The evaporator is a cross-flow finned tube heat exchanger with about 10% more area than models presently on the market, and this sizing gave a mean evaporative temperature difference of about 6.5°F for the R-410A case. The HPWH assumes 300 CFM airflow across the evaporator with 30 watts of fan power, which also implies a BPM motor. The R410A HPWH design were optimized for heating COP at an assumed average EWT of 115°F and at the fixed 67.5°F DB, 50% RH inlet air condition of the DOE UEF test.

Therefore, in the design of a comparable transcritical CO₂ HPWH, the heat exchanger sizes were adjusted to obtain the same mean temperature differences designed in the R-410A case. The pump and fan power and airflow assumptions were consistent with those used for the R410A case mentioned above. For the compressor, we adopted a relatively high efficiency reciprocating model for which we could obtain a performance map comparable to those for the HFC refrigerant compressors, as no rotary CO₂ compressor performance maps could be obtained for this analysis. The overall isentropic efficiency of the CO₂ compressor is 15% less than the rotary R410A compressor (Baxter et.al. 2011) at rated cooling conditions. A once-through design for the water flow was assumed for the primary CO₂ HPWH system to obtain best matching of the water and refrigerant temperature glides in the gas cooler. In the once-through design, a fixed 140°F return water temperature was maintained by adjusting the pump flow and power assuming a BPM pump.

Figure 3 show the steady-state performance of COP and heat capacity of R410A and CO₂ systems with the same mean temperature differences of condenser and evaporator calibrated at EWT of 115°F and 67°F DB, 50% RH inlet air conditions. The COP of R410A is significantly higher than CO₂, and the heating capacity of R410A is also higher than the comparable CO₂ system. The lower heating capacity of the CO₂ HPWH is mainly due to the small compressor displacement. The lower COP of the CO₂ HPWH is probably due to the lower overall isentropic efficiency and the higher compressor heat loss ratio (i.e., $\eta_{\text{loss}} = 0.45$), leading to higher electric energy consumption and lower CO₂ discharge enthalpy at compression process, respectively. Our simulations reflect that the overall isentropic efficiency of the CO₂ compressor is 0.52 compared to the R410A compressor of 0.58 at EWT of 115 °F and 67 °F DB, 50% RH inlet air conditions. This is a 10.3% lower isentropic efficiency at water heating conditions. This indicates that it is vital for CO₂ HPWH to continuously improve compressor efficiency via novel component design. On the other hand, the system optimization is also vital. Figure 4 shows that different CO₂ HPWH calibration design will substantially affect the COP and heating capacity with different overall heat transfer coefficients and mean heat transfer temperature difference.

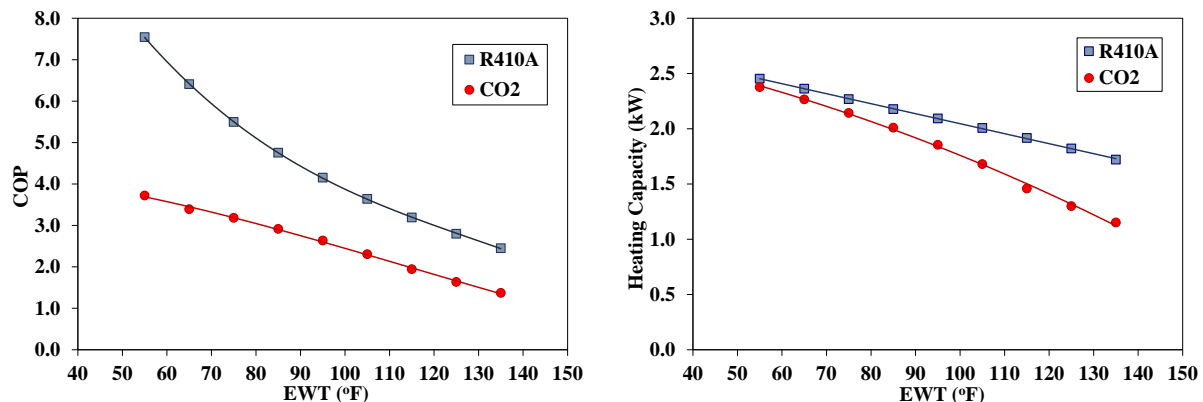


Figure 3: Comparison of COP and heat capacity between R410A and CO₂ systems calibrated at the same mean temperature differences of condenser and evaporator for EWT of 115°F and 67°F DB, 50% RH inlet air conditions.

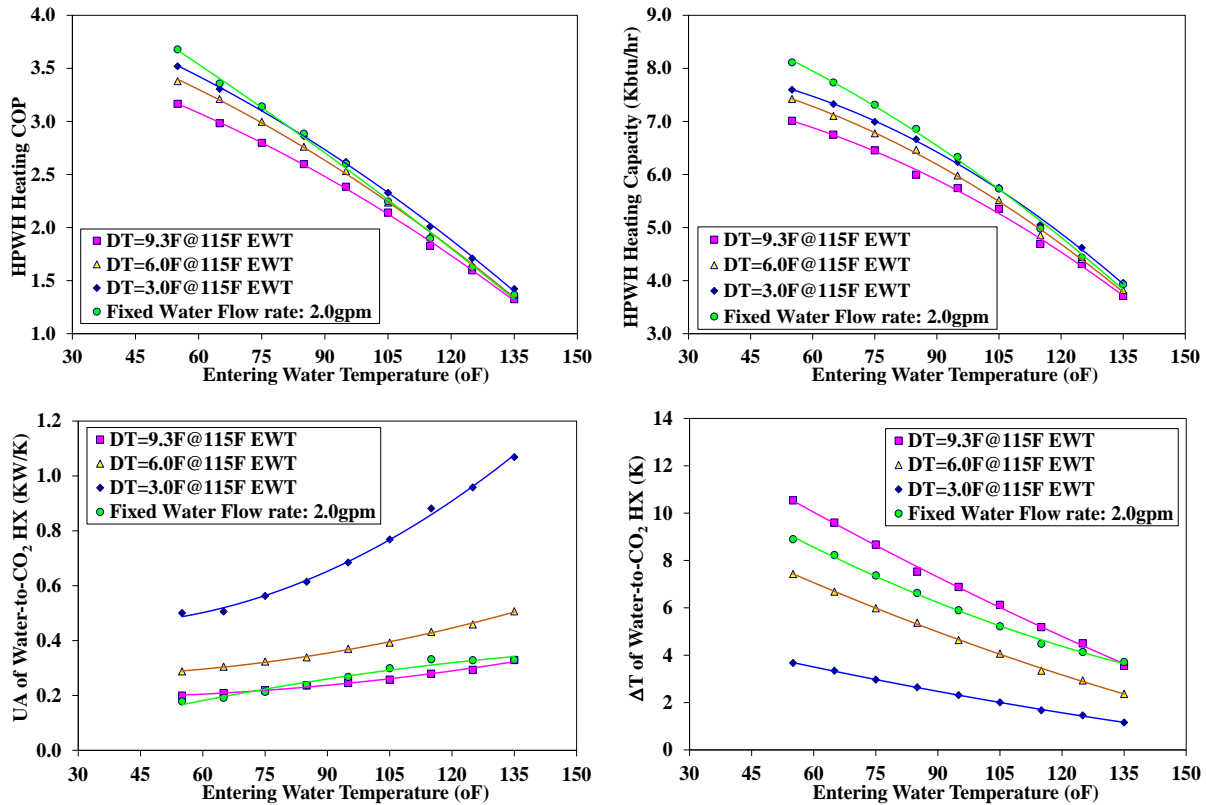


Figure 4: Impact of CO₂ HPWH calibration design on COP, heating capacity, UA and mean temperature difference.

The performance maps along with the water flow rates (Baxter et.al. 2011) were used in TRNSYS to carry out 24-hour UEF simulation. The results are shown in Table 2. This simulation included a nominal 50-gallon water tank model (actual assumed capacity of 45 gallons), divided into 6 equal volume regions from top (zone 1) to bottom (zone 6). During the first 6 hours, 10-gallon hot water each hour is drawn from the zone 1 with 3.0 gpm. Two HPWH heat-up modes were chosen to compare the UEFs between R410A and CO₂ HPWHs. One of a typical HPWH heat-up mode is a stepwise heat-up, where the water was removed from node 6 and returned to node 5 with small temperature rises on each pass. The other is the once-thru cases, where the water is removed from node 6, heated in one pass of HPWH, and returned to node 1. The primary HPWH control locations are at node 5 for the stepwise heat-up cases and node 2 for the once-thru designs. To account for tank heat losses, ORNL UEF calculations assumed that tank insulation for these analyses gives a 0.90 UEF for a tank heated with electric resistance elements. The once-thru heat up method can improve CO₂ HPWH UEF, but the CO₂ HPWH still achieves less UEF than the comparable R410a unit.

Table 2. Numerical comparison of R410A and CO₂ HPWH designs (Data source: Baxter et.al. 2011)

Case	Refrigerant	Heatup method	EWT (°F)	UEF _{0.9}
1	R410A	Stepwise	114.3	2.84
2	CO ₂	Stepwise	110.5	2.02
3	CO ₂	One-thru	92.0	2.34
4	CO ₂	One-thru	82.9	2.57
5	CO ₂ w/ LSHX	One-thru	82.9	2.66

The studies described above are focused on residential hot water supply applications not exceeding 140°F in the United States. However, CO₂ HPWH systems typically operate in supercritical conditions, resulting in an effective heat transfer to lift the water temperature up to 194°F or 248 °F (90°C or 120°C). In such hot water applications, the performance and efficiency of the conventional refrigerants degrade. Therefore, CO₂ HPWHs still have good potential applications, particularly in commercial hot water supply, which usually requires over 194°F.

4. CONCLUSIONS

An air-source CO₂ HPWH simulation model was developed based on ACMODEL design model combined with the component models developed at ORNL. The updated model was used to evaluate the potential of a residential CO₂ HPWH designed under US residential application standards, as well as in guiding the state-of-art CO₂ HPWH designs by using numerical simulation. In the study, we simulated CO₂ HPWH performance and compared with the heat pump water heater using conventional refrigerants. The results show that, compared to conventional refrigerants, the current CO₂ HPWH component and system technology results in a lower efficiency performance in the application of U.S. residential hot water supply not exceeding 140°F. Therefore, it is vital for CO₂ HPWHs to continuously improve compressor and system efficiency via novel component design. On the other hand, CO₂ HPWHs still have good potential applications in commercial hot water supply, which usually requires over 194°F.

REFERENCES

1. Aprea, C., Maiorino, A. (2008). An experimental evaluation of the transcritical CO₂ refrigerator performances using an internal heat exchanger. *International journal of refrigeration*, 31, 1006–1011
2. Baxter, V.D., Murphy, R.W., Rice, C.K., Shen, B., Gao, Z. (2011). Analysis of Highly Efficient Electric Residential Heat Pump Water Heaters for Cold Climates. ORNL/TM-2011/278, 2011.
3. Beaver, A., Hrnjak, P., Yin, J., Bullard, C. (2000). Effects of distribution in headers of microchannel evaporators on transcritical CO₂ heat pump performance. *The ASME Advanced Energy Systems Division, AES-Vol. 40*, New York, 55-64.
4. Chang, Y.J., Wang, C.C., Chang W.J. (1994). Heat transfer and flow characteristics of automotive brazed aluminum heat exchangers. *ASHRAE Transactions: Symposia*, 643 - 652.
5. Chen, J.P., Liu, J.P., Chen, Z.J., Niu, Y.M. (2004). Trans-critical R744 and two-phase flow through short tube orifices. *International Journal of Thermal Science*, 43, 623-630.
6. Cheng, L., Ribatski, G., Thome, J.R. (2008). Analysis of supercritical CO₂ cooling in macro- and micro-channels. *International Journal of Refrigeration*, 31, 1301-1316.
7. Dittus, F.W., Boelter, L.M.K. (2010). *Publications on Engineering*, 2, University of California, Berkeley, pp443.
8. Embraco. Compressor Technical Data. Update at 18 Aug. 2010.
9. Fartaj, D., Ting, S.-K., Yang, W.W. (2004). Second law analysis of the transcritical CO₂ refrigeration cycle. *Energy Conversion and Management*, 45(13-14), 2269-2281.
10. Gao, Z., Mei, V.C., Chen, F.C. (2003). CFD solution and experimental testing of buoyancy-driven convection caused by condensers immersed in a water tank of HPWH. *ASME International Mechanical Engineering Congress and Exposition*, Vol. 37084, 33-38.
11. Gao, Z. (2010). The impact of thermostatic expansion valve heating on the performance of air-source heat pumps in heating mode. *Energy conversion and management*, 51(4), 732-739.
12. Groll, E.A., Kim, J.-H. (2007). Review of recent advanced toward transcritical CO₂ cycle technology. *HVAC&R Research*, 13(3), 499-520.
13. He, Y. J., Liang, X. Y., Cheng, J. H., Shao, L. L., Zhang, C. L. (2020). Approaching optimum COP by refrigerant charge management in transcritical CO₂ heat pump water heater. *International Journal of Refrigeration*, 118, 161-172.
14. Hugelmann, R.D. (2004). Performance study of a 2-ton residential CO₂ A/C system with a variable flow rate CO₂ compressor. *International Compressor Engineering Conference*, July 12-15, Purdue.
15. Huff, H.-J., Radermacher, R (2003). CO₂ compressor-expander analysis. ARTI-21CR/611-10060-01.
16. Hwang, Y., Radermacher, R. (1998). Theoretical evaluation of carbon dioxide refrigeration cycle. *HVAC&R Research*, 4(3), 245–63.
17. Jakobsen, A., Skiple, T., Nekså, P., Wachenfeldt, B., Stene, J., Skaugen, G. (2006). Development of reversible residential air conditioners and heat pump using CO₂ as working fluid. *IEA Heat Pump Centre newsletter*, 24(3).
18. Kandlikar, S.G. (1990). A general correlation for saturated two-phase flow boiling heat transfer inside horizontal and vertical tubes. *ASME Journal of Heat Transfer*, 112, 219 – 228.
19. Kim, M.-H., Pettersen, J., Bullard, C.K. (2004). Fundamental process and system design issues in CO₂ vapor compression systems. *Progress in Energy and Combustion Science*, 30, 119-174.

20. Li, D., Groll, E.A. Transcritical CO₂ refrigeration cycle with ejector-expansion device. *International Journal of Refrigeration*, 28, 766–773.
21. Liao, S.M., Zhao, T.S., Jakobsen, A. (2000). A correlation of optimal heat rejection pressures in transcritical carbon dioxide cycles. *Applied Thermal Engineering*, 20, 831-841.
22. Liu, F., Groll, E.A. (2008). Recovery of throttling losses by a two-phase ejector in a vapor compression cycle, ARTI Report No. 10110-01.
23. Nawaz, K., Shen, B., Elatar, A., Baxter, V., Abdelaziz, O. (2018). Performance optimization of CO₂ heat pump water heater. *International Journal of Refrigeration*, 85, 213-228.
24. Nekså, P. (2002). CO₂ heat pump systems. *International journal of refrigeration*, 25 421-427.
25. Nekså, P., Rekstad, H., Zakeri, G.R., Schiefloe, P.A. (1998). CO₂-heat pump water heater: characteristics, system design and experimental results, *International Journal of Refrigeration*, 21, 172-179.
26. Ortiz, T.M., Li, D., Groll, E.A. (2003). Evaluation of the performance potential of CO₂ as a refrigerant in air-to-air conditioners and heat pumps: system modeling and analysis. ARTI-21CR/610-10030.
27. Park, C.Y., Hrnjak, P.S. (2007). CO₂ and R410A flow boiling heat transfer, pressure drop, and flow pattern at low temperatures in a horizontal smooth tube, *International Journal of Refrigeration*, 30, 166-178.
28. Richardson, D.H., Aute, V., Winkler, J., Radermacher, R. (2004). Numerical challenges in simulation of a generalized vapor compression refrigeration system. 2004 International Refrigeration and Air Conditioning Conference, Purdue.
29. Pettersen, J., Rieberer, R., Munkejord, S.T. (2000). Heat transfer and pressure drop for flow of supercritical and subcritical CO₂ in microchannel tubes. SINTEF Energy Research Technical Report TR A5127.
30. Peuker, S., Hrnjak, P. (2006). R744 two evaporator system for US army HMMWV, International Refrigeration and Air Conditioning Conference, Purdue.
31. Richardson, D.H., Jiang, H., Lindsay, D., Radermacher, R. (2002). Optimization of vapor-compression systems via simulation. 2002 International Refrigeration and Air Conditioning Conference, Purdue.
32. Richter, M.R., Bullard, C.W., Hrnjak, P.S. (2001). Comparison of R744 and R410a for residential heating and cooling applications, ACRC CR-39.
33. Richter, M.R., Song, S.M., Yin, J.M., Kim, M.H., Bullard, C.W., Hrnjak, P.S. (2003). Experimental results of transcritical CO₂ heat pump for residential application. *Energy*, 28, 1005-1019.
34. Rigola, J., Raush, G., Pérez-Segarra, C.D., Oliva, A. (2005). Numerical simulation and experimental validation of vapour compression refrigeration systems. Special emphasis on CO₂ trans-critical cycles, *International Journal of Refrigeration*, 28(8), 1225-1237.
35. Stene, J. (2005). Residential CO₂ heat pump system for combined space heating and hot water heating, *International Journal of Refrigeration*, 28, 1259–1265.
36. Wang, C.C., Lin, Y.T., Lee, C.J. (2000). Heat and momentum transfer for compact louvered fin-and-tube heat exchangers in wet conditions. *International Journal of Heat and Mass Transfer*, 43, 3443 – 3452.
37. Yang, J.L., Ma, Y.T., Lia, M.X., Guan, H.Q. (2005). Exergy analysis of transcritical carbon dioxide refrigeration cycle with an expander. *Energy*, 30(7), 1162-1175.
38. Ye, Z., Wang, Y., Song, Y., Yin, X., & Cao, F. (2020). Optimal discharge pressure in transcritical CO₂ heat pump water heater with internal heat exchanger based on pinch point analysis. *International Journal of Refrigeration*, 118, 12-20.
39. Yin, J.M., Bullard, C.W., Hrnjak P.S. (2001). R-744 gas cooler model development and validation. *International Journal of Refrigeration*, 24, 692 – 701.

ACKNOWLEDGEMENT

This research used resources at the Building Technologies Research and Integration Center, a DOE Office of Science User Facility operated by ORNL. We also thank our colleagues who provided helps in the work.

This manuscript has been authored by UT-Battelle, LLC, under contract DE-AC05-00OR22725 with the US Department of Energy (DOE). The publisher acknowledges the US government license to provide public access under the DOE Public Access Plan (<http://energy.gov/downloads/doe-public-access-plan>).